JOURNAL OF GEOPHYSICAL RESEARCH: SOLID EARTH, VOL. 118, 22–38, doi:10.1029/2012JB009605, 2013

# Methane release from warming-induced hydrate dissociation in the West Svalbard continental margin: Timing, rates, and geological controls

K. E. Thatcher,[1,2] G. K. Westbrook,[1,3,4] S. Sarkar,[3] and T. A. Minshull[3]

Received 5 July 2012; revised 18 October 2012; accepted 5 November 2012; published 30 January 2013.

[1] Hundreds of plumes of methane bubbles, first observed in 2008, emanate from an area of the seabed off West Svalbard that has become 1°C warmer over the past 30 years. The distribution of the plumes, lying close to and upslope from the present upper limit of the methane hydrate stability zone, indicates that methane in the plumes could come from warming-induced hydrate dissociation, a process commonly invoked as contributing to rapid climate change. We used numerical modeling to investigate the response of hydrate beneath the seabed to changes in bottom-water temperature over periods of up to 1000 years B.P. The delay between the onset of warming and emission of gas, resulting from the time taken for thermal diffusion, hydrate dissociation, and gas migration, can be less than 30 years in water depths shallower than the present upper limit of the methane hydrate stability zone, where hydrate was initially several meters beneath the seabed and fractures increase the effective permeability of intrinsically low-permeability glacigenic sediment. At the rates of warming of the seabed that have occurred over the past two centuries, the enthalpy of hydrate dissociation limits the rate of gas release to moderate values. Cycles of warming and cooling can create and sustain hydrate close to the seabed where there is locally a supply of methane of tens of mol·m$^{-2}$ yr$^{-1}$. This rate of gas flow can be achieved where stratigraphic and structural heterogeneity focus gas migration, although the regional rate of methane supply could be much less.

**Citation:** Thatcher, K. E., G. K. Westbrook, S. Sarkar, and T. A. Minshull (2013), Methane release from warming-induced hydrate dissociation in the West Svalbard continental margin: Timing, rates, and geological controls, *J. Geophys. Res. Solid Earth*, *118*, 22–38, doi:10.1029/2012JB009605.

## 1. Introduction

[2] The release of methane to the atmosphere from methane hydrate in sediment beneath the ocean floor has been invoked as a contributing agent to rapid climate-warming events in the past, such as the Palaeocene-Eocene Thermal Maximum [*Dickens et al*., 1995] and Quaternary glacial-to-interglacial transitions [*Kennett et al*., 2003]. A current concern is that modern climate warming will destabilize methane hydrate, releasing methane into the water column and from there to the atmosphere. Methane is about 70 times more powerful in its effect as a greenhouse gas on warming than is carbon dioxide over a period of 20 years [*Forster et al*., 2007], and a substantial increase in methane released from hydrate could reinforce global warming.

[3] Hydrate is stable under conditions of low temperature and high pressure. In the Arctic, colder water at the seabed allows hydrate to form in shallower water than elsewhere. If sediment that contains hydrate is warmed sufficiently, the hydrate will dissociate to produce methane gas and water. Hydrate in shallow water and at a shallow depth beneath the seabed will be affected by climate warming earliest and most strongly [*Archer et al*., 2009]. Because the Arctic is predicted to experience the most intense warming over this century [*Hassol*, 2004], the Arctic is particularly vulnerable to dissociation of hydrate.

[4] As a consequence of the increasing temperature of Atlantic water flowing into the Arctic, a large part of the seabed in the depth range 350–600 m could be prone to the release of methane over the next 100 years, if underlain by sediment containing hydrate [*Biastoch et al*., 2011]. Abundant methane in the water column of parts of the East Siberian Arctic continental shelf, some of which enters the atmosphere, is attributed to the continuing marine flooding and consequent warming of a former land surface underlain by permafrost [*Shakhova et al*., 2010a, 2010b], although it seems unlikely that an increase in the rate of warming over

[1]School of Geography, Earth and Environmental Sciences, University of Birmingham, Birmingham, UK.
[2]Department of Earth Sciences, University of Durham, Durham, UK.
[3]National Oceanography Centre Southampton, University of Southampton, European Way, Southampton, UK.
[4]Géosciences Marines, Ifremer Centre de Brest, Plouzané, France.

Corresponding author: G. K. Westbrook, School of Geography, Earth and Environmental Sciences, University of Birmingham, Birmingham, B15 2TT, UK. (g.k.westbrook@bham.ac.uk)


2169-9313/13/2012JB009605

the last 25 years or so has yet had any significant effect on hydrate in permafrost [*Dmitrenko et al.*, 2011]. Off western Svalbard, where glacial ice withdrew from the continental shelf about 13 ka [*Landvik et al.*, 2005], warming of the uppermost part of the continental slope by the increasing temperature of the West Spitsbergen current appears to have induced the release of methane from the dissociation of subseabed hydrate. Temperature measurements from conductivity-temperature-depth casts over the 33 year period from 1975 until 2008 show a 1°C warming of the bottom water in the range 300–450 m water depth [*Westbrook et al.*, 2009].

[5] Sonar images obtained from the West Svalbard margin [*Westbrook et al.*, 2009] in Autumn 2008 showed hundreds of bubble plumes (flares) emanating from the seabed. Water samples taken from the plumes contained concentrations of dissolved methane that were up to 20 times higher than background. The gas flares are most numerous in a zone about a kilometer wide, extending upslope from a depth of about 400 m to the continental shelf (Figures 1 and 2), which is covered by glacially derived sediment [*Sarkar et al.*, 2011a; *Rajan et al.*, 2012]. The flares also occur, but more sparsely distributed, farther east in shallower water, where the gas feeding them does not come directly from hydrate dissociation, because the seabed is well outside the methane hydrate stability zone (MHSZ). The landward limit of the MHSZ in seawater at its present-day temperature of 3°C lies at a depth of approximately 400 m. With the exception of two flares at 407 m depth, flares do not occur in water depths greater than 400 m in this area. It is probable that the distribution of the flares could be explained by the dissociation of hydrate that previously occurred beneath the seabed between 370 and 400 m water depth, induced by warming of 1°C over the past 30 years or so, leading to a release of methane into the ocean (Figure 3, inset). Although gas migrating from beneath the MHSZ could be the source of gas feeding flares in water depths shallower than 370 m, it cannot be the only source of gas emissions from the seabed between 370 and 400 m water depth. The presence of the MHSZ beneath the seabed in this depth range 30 or more years ago, would have caused any methane migrating into it to form hydrate, which subsequently dissociated from the effect of warming of the seabed [*Westbrook et al.*, 2009].

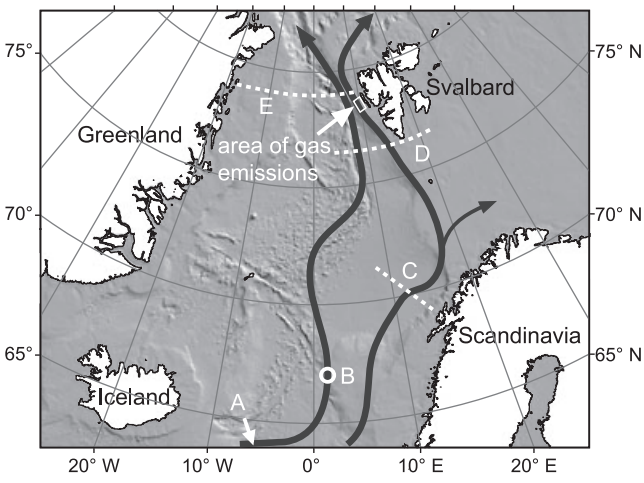


**Figure 1.** Position of the area of occurrence of methane bubble plumes off western Svalbard in the northeastern Atlantic Ocean (see Figure 2) and the major pathways of Atlantic inflow water to the Arctic from the eastern subpolar gyre. Adapted from [*Holliday et al.*, 2008]. Letters show the locations of temperature-time series shown in Figure 9.

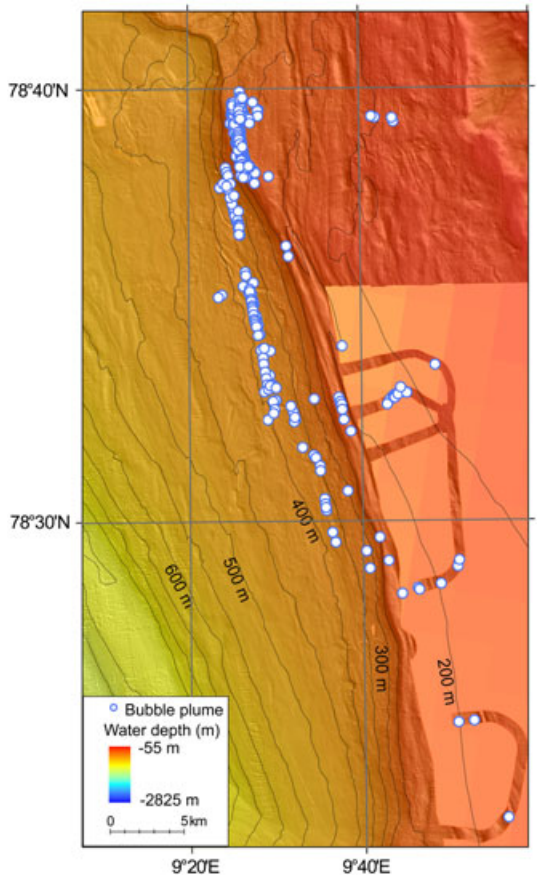


**Figure 2.** Bathymetric map of the zone of bubble plumes. Individual plumes observed in 2008 are indicated by blue circles filled in white. Contours are at 50 m intervals. The map is derived from multibeam echo-sounding data acquired on Cruise JR211 of RRS *James Clark Ross* and, in the NE corner, data from the Norwegian Hydrographic Service.

[6] In the vicinity of the gas flares, there are numerous negative polarity seismic bright spots and scatterers shown in the seismic reflection sections, some of them immediately beneath the individual sites of flares [*Sarkar et al.*, 2011b; *Rajan et al.*, 2012; *Sarkar et al.*, 2012]. Farther downslope, multichannel seismic reflection and ocean-bottom seismometer data show numerous indications of the presence of gas at the base of the MHSZ, forming a bottom-simulating reflector (BSR), and at depths greater than the expected base of the MHSZ [*Westbrook et al.*, 2008]. These latter include strong negative polarity reflections, underlain by zones of strong attenuation and decreased *P*-wave velocity with no decrease in *S*-wave velocity [*Chabert et al.*, 2011]. The overall situation is one in which free gas migrates upslope through permeable units in a sequence of seaward-dipping marine sediments, which underlies glacigenic deposits in the shallower water of the upper part of the continental slope and the shelf (Figure 3). Gas flares occur above the subcrops of gas-rich units in this sequence beneath the glacigenic cover on the shelf. Gas also finds its way into the glacigenic

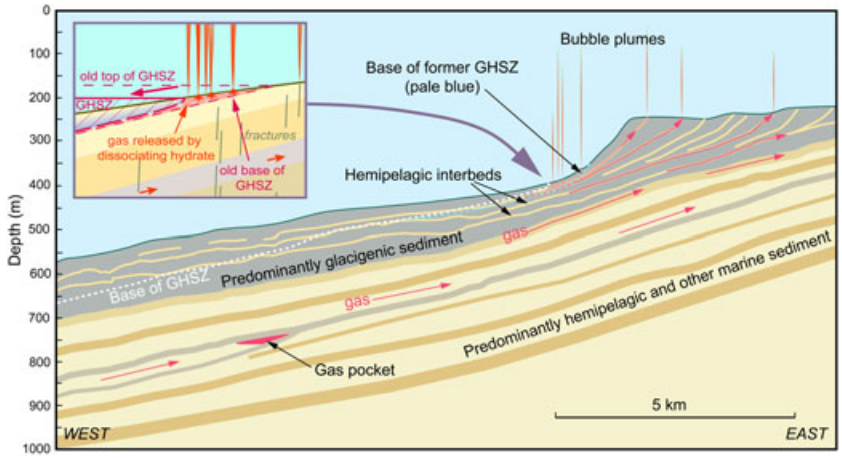


**Figure 3.** Summary cross-section depicting the uppermost part of the continental margin of western Svalbard, based on seismic and sonar data [*Chabert et al*., 2011; *Sarkar et al*., 2011b, 2012]. The calculated present-day base of the MHSZ is shown by the white dashed line and its calculated base in 1978 is shown by the pale blue dashed line. Inset is an illustration of the processes active in the vicinity of the outcrop of the base the MHSZ at the seabed. There is abundant evidence of gas migrating upslope from sources deep beneath the MHSZ and feeding gas seeps at the edge of the shelf.

sediment sequence on the upper part of the slope, where it occupies stratigraphic units within the sequence, presumably hemipelagic interbeds deposited during interglacial periods, and in water depths shallower than 400 m depth, gas migrates to the seabed. The exact nature of the pathways of gas migration across the stratigraphic units is not shown by the seismic data, although there are numerous near-vertical zones of locally reduced seismic amplitude [*Sarkar et al*., 2011b; *Rajan et al*., 2012]. The pathways are likely to be cracks. Farther downslope, seismic anisotropy displayed by *PS* converted waves indicates the presence of aligned near-vertical cracks in the shallow sedimentary sequence [*Haacke and Westbrook*, 2006; *Haacke et al*., 2009] and the position of the glacigenic sequence at the top of the continental slope makes it prone to the development of cracks created by gravitationally induced tensile stress acting downslope [e.g., *Driscoll et al*., 2000; *Sultan et al*., 2004; *Micallef et al*., 2008]. The widespread evidence for free gas in the sediment together with the restriction of the occurrence of gas flares to the area landward of the limit of the MHSZ make it highly probable that some hydrate occupies the shallow MHSZ beneath the seabed downslope from its landward limit and that hydrate previously occurred beneath the seabed in the area from which the MHSZ withdrew as seabed temperature increased over the last 30 or so years.

[7] In this paper, we investigate the hypothesis that the methane in the plumes is derived from hydrate dissociated by ocean warming. We do so by examining, through numerical simulations, the dependence of the time lag between warming of the seabed and the emission of gas from the seabed, and the rate of emission of gas upon:

1) The distribution and concentration of the hydrate in the sediment;
2) The type and distribution of permeability in the sedimentary section containing the hydrate;
3) The input of methane into the base of the system.

[8] In addition, we explore the effect of probable histories of seabed-temperature variation on gas release and on the distribution of hydrate in the hydrate stability zone.

## 2. Modeling Approach

[9] Numerical modeling of fluid flow and heat flow coupled with hydrate formation and dissociation was undertaken with TOUGH+Hydrate [*Moridis et al*., 2008]. TOUGH+Hydrate has been used previously to investigate the fate of oceanic hydrate under a warming ocean, for both one-dimensional (1D) and two-dimensional (2D) cases [*Reagan and Moridis*, 2008, 2009; *Reagan et al*., 2011; *Thatcher and Westbrook*, 2011]. The 2D case [*Reagan and Moridis*, 2009; *Reagan et al*., 2011] was based on the West Svalbard situation, confirming the feasibility of warming-related hydrate dissociation proposed for this location [*Westbrook et al*., 2009], but did not employ the detailed geological and geophysical information that has been used to inform the modeling presented here. 2D models are informative about the effect of the slope of the seabed on where gas flows and emerges at the seabed. In the upper slope, however, between 550 and 350 m water depth, the slope is 1° (Figure 2). The 2D models of *Reagan et al*. [2011], with a slope of nearly 3°, have uniform intrinsic properties (excluding the effects of hydrate and free gas). In reality, the subsurface geology is layered, with different sediment types and is also horizontally heterogeneous [*Rajan et al*., 2012; *Sarkar et al*., 2012]. The effects of vertical and horizontal heterogeneity of properties outweigh the effect of slope where the slope is very small. The horizontal component of head gradient introduced by a 1° slope in an aquifer is about 2% of the vertical gradient. This could give large lateral flows of gas over long uninterrupted flow paths, as is probably the case in the deeper marine sequence, but in the shallow sediment, dominated by glacigenic sediments, heterogeneity of permeability between marine, and glacigenic sediments will act to restrict lateral flow. Furthermore,

*Reagan et al.* [2011] note that the error in the 1D approximation, by comparison with 2D, is very small for low hydrate saturation. For these reasons, and because initialization and run times of 2D models were too long to permit a large number of runs for sensitivity testing, we adopted a 1D approach. Essentially, the 1D model represents the zone beneath an individual gas plume, and should, in time, yield a flow of free gas at the seabed, given the appropriate properties and initial conditions.

[10] The models were run for a range of water depths between 380 and 410 m (Figure 4). The basic 1D model has a cell thickness of 0.5 m for the first 100 m depth and thereafter cell thickness increases by a factor of 1.1 for each successive cell to a maximum depth of 1134 m. Cells of thickness 0.001 m at the top and bottom of the model are used for boundary conditions and there is no flow in the horizontal ($x$ and $y$) directions. Flow is in the vertical ($z$) direction, only. The bottom cell has a source term that is used to represent fixed heat and fluid flows. The top cell of the model represents the bottom of the ocean, with a prescribed pressure, temperature, and aqueous methane saturation. The models were initialized with a hydrostatic pressure gradient and constant heat flow. The base of the hydrate stability zone was found by the code during initialization, using the hydrate stability criterion from [*Moridis*, 2003] for pore water containing sodium chloride at a concentration of 35 $g \cdot kg^{-1}$. This stability criterion is very close (equivalent to within less than 4 m of predicted water depth for the same temperature) to that of *Sloan and Koh* [2008], derived from minimization of Gibbs free energy with the CSMGem code. The values of the invariant model parameters are listed in Table 1.

[11] The average geothermal gradient in the area was estimated at 65 $°C \cdot km^{-1}$ from observations of the depths of the BSR in seismic reflection data nearby (about 8 km distant) [*Sarkar et al.*, 2011b, 2012]. The thermal conductivity and diffusivity of water-saturated sediments were calculated for sediment porosity of 60%, using the method of *Budiansky* [1970], and multiplied by the average geothermal gradient to derive heat flow. Because thermal gradient changes when pore space contains hydrate rather than water, constant heat flow is required for the initial condition rather than a constant thermal gradient. Intrinsic (absolute) permeability in the model was assumed to be uniform, and different models took a range of values of permeability across seven orders of magnitude. The presence of hydrate reduces the permeability, depending upon its concentration. This is implemented in the model through a reduction in gas and water saturation, as hydrate also occupies pore space, leading to a reduction in relative permeability. The presence of fractures introduces a dual porosity-permeability system. Where fractures predominate, the properties of the system approximate to those of the fracture network, with high permeability and low porosity, and, in cases where this was considered to be probable, layers were given a very low porosity (1%) and high permeability ($10^{-12}$ $m^2$) to simulate the properties of a fracture network. The definitions of relative permeability and capillary pressure are taken from *Van Genuchten* [1980] and *Stone* [1970], respectively. For gas saturations equal or less than the irreducible gas saturation, the relative permeability of gas is zero. The default value for irreducible gas saturation (2%) follows other modeling studies of gas-water-hydrate systems and laboratory measurements [*Liu and Flemings* 2007; *Reagan and Moridis*, 2008, 2009; *Reagan et al.*, 2011; *Yousif et al.*, 1991]. We tested the sensitivity of the models to this parameter because it determines how much gas must be produced before flow starts.

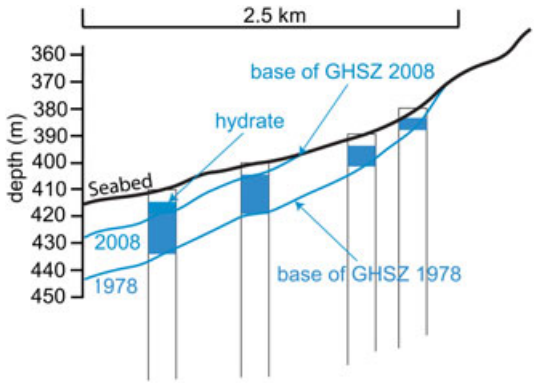


**Figure 4.** Schematic representation of the modeling scheme, showing the sequence of 1D models, each of which extend to a depth of 1134 m below the sea bed, in relation to the calculated positions of the MHSZ in 1978 and 2008. The results from the model for a water depth of 390 m are used as the primary illustration of the response of the system where the seabed is no longer in the MHSZ in 2008.

[12] Changes in bottom-water temperature with time were applied to the model at yearly intervals by changing the temperature in the upper boundary cell. Methane flow into this cell was taken to represent methane flow into the ocean, and the time lag between the onset of warming and the start of the flow of gaseous methane into the top cell was recorded. This lag should be less than 33 years if the gas bubbles observed in 2008 were a consequence of warming of the seabed since 1975.

## 3. Results

### 3.1. Response to a Linear Increase in Temperature

[13] The primary elements of the response to warming are illustrated by a model of hydrate dissociation as the seabed temperature at 390 m depth warms linearly from 2 to 3°C over a period of 33 years and then remains constant at 3°C until 100 years (Figure 5). The depth at which the deepest large group of flares cluster is 390 m, just landward of the predicted limit of the MHSZ and where the delay between the onset of warming and the emission of gas from the seabed would be greatest (Figure 2). The permeability used for the initial model is $10^{-13}$ $m^2$. This is higher than that of the intrinsic permeability of fine-grained clay-rich sediment, which would typically be about $10^{-15}$ $m^2$. We explore the effects of varying permeability and discuss, below, why this higher permeability is likely to be more representative of the effective permeability of the sediments here than their intrinsic permeability. The base of the hydrate stability field is initially at 402 m depth (12 m beneath the seabed). The top of the hydrate stability zone in the water column is initially at 372 m depth and after 16 years it reaches the seabed. Hydrate initially occupies the interval between 7 and 12 m beneath the seabed. Gas reaches the seabed 38 years after warming starts. After 5 years, warming at the base of the hydrate stability zone has started to cause dissociation of

**Table 1.** Base Case Model Parameters. $k_{rA}$ and $k_{rG}$ are Relative Permeabilities for Aqueous and Gaseous Phases Respectively; $S_A$ and $S_G$ are Aqueous and Gas Saturations and $S_{mxA}$ is the Maximum Water Saturation; $S_{irA}$ and $S_{irG}$ and Irreducible Saturations of Aqueous Solution and Gas; $P_{cap}$ is Capillary Pressure, $P_0$ is the Capillary Entry Pressure, $P_{max}$ is the Maximum Value of Capillary Pressure, $n$ and $\lambda$ are Fitting Parameters

| Parameter | Value |
|---|---|
| Initial hydrate saturation | 5% |
| Initial salinity | 0.035 wt % |
| Ocean warming | $0.03^{\circ}C \cdot yr^{-1}$ for 33 years |
| Gas Composition | 100% $CH_4$ |
| Water saturated thermal conductivity | 1.21 $Wm^{-1}$ $K^{-1}$ |
| Sediment density | 2600 $kg^{-1}$ $m^3$ |
| Heat flow (initially constant) | $7.865 \times 10^{-2}$ $W \cdot m^{-2}$ |
| Porosity | 60% |
| Permeability | $10^{-13}$ $m^2$ |
| Relative permeability | $k_{rA} = \max\left\{0, \min\left\{\left[\frac{S_A - S_{irA}}{1 - S_{irA}}\right]^n, 1\right\}\right\}$ |
| (Modified version of Stone's first three phase relative permeability method [*Stone*, 1970]) | $k_{rG} = \max\left\{0, \min\left\{\left[\frac{S_G - S_{irG}}{1 - S_{irA}}\right]^n, 1\right\}\right\}$ |
| | $S_{irA} = 0.12, S_{irG} = 0.02, n = 4$ |
| Capillary pressure [*van Genuchten*, 1980] | $P_{cap} = -P_0\left[(S^*)^{-1/\lambda} - 1\right]^{-\lambda}$ |
| | $-P_{max} \le P_{cap} \le 0$ |
| | $S^* = \frac{(S_A - S_{irA})}{(S_{mxA} - S_{irA})}$ |
| | $\lambda = 0.254, S_{irA} = 0.11, P_0 = 12500$ MPa |
| | $P_{max} = 10^6$ MPa, $S_{mxA} = 1$ |

hydrate to methane gas and fresh water. At 20 years, hydrate dissociation is occurring through the entire layer containing hydrate and the heat energy is being used for dissociation of hydrate rather than warming deeper sediments. Gas and hydrate occur together, because as dissociation occurs, the increase in pressure caused by released gas (Figure 5c) and the salinity decrease caused by released water (Figure 5e) both increase the stability of hydrate, which is continually compensated by an increase in temperature up to the temperature at which hydrate dissociates at decreased salinity and increased pressure. For 35 years, the geotherms in the region where hydrate is present (Figure 5a) remain tightly bunched, close to the dissociation temperature, because the presence of hydrate buffers the temperature at its dissociation temperature, which gradually increases, as pressure increases and salinity decreases. Once the hydrate has dissociated, the geotherms migrate rapidly toward the long-term geotherm appropriate for the increased temperature of the seabed. Whilst hydrate is present, gas flow is restricted by reduced permeability caused by the hydrate, but permeability increases as the hydrate dissociates. Consequently, gas pressure reduces significantly and gas reaches the seabed just after the hydrate has finished dissociating at about 38 years (Figures 5b, 5c, and 5d). Thereafter, gas in pore space asymptotically declines toward its irreducible gas saturation of 2% (Figure 5d).

[14] The controls on the length of the time delay between the onset of warming and the appearance of gas at the seabed, were explored by varying permeability, porosity, hydrate saturation, critical gas saturation, and the depth to the top of a 5 m thick hydrate layer while keeping the initial ocean temperature, water depth, and hence hydrate stability zone constant. The delay decreases with increasing permeability due to the shorter time taken for gas to flow to the seabed (Figure 6a) and vice versa. Furthermore, when permeability is low gas pressure increases as hydrate dissociates, making the hydrate stable and inhibiting further dissociation until pressure dissipates or temperature increases. For permeability less than $10^{-16}$ $m^2$, the increased pressure is so great that lithostatic pressure is exceeded within 25 years, by which time fracturing would have occurred in the sediment and flow would no longer be primarily through its matrix, but through a network of cracks, with a consequent large increase in permeability. For the case in which hydrate is at the seabed, the delay is 16 years, which is the minimum delay, representing the time for the seabed at this water depth to move out of the hydrate stability zone, as the water becomes warmer. The minimum delay is less in shallower water, where the seabed is closer to the initial top of the MHSZ. The delay increases as the depth of the top of the hydrate beneath the seabed increases, because of the greater distance over which heat has to diffuse downward and gas liberated from hydrate has to flow upward. Decreasing porosity reduces the delay (Figure 6b), because the gas produced has a smaller volume to fill and, therefore, irreducible gas saturation is reached earlier and gas starts to flow sooner.

[15] The amount of hydrate in the pore space has little effect on the time at which methane appears at the seabed, except when there is only a small amount of hydrate and permeability is low (Figure 6c). Models with 2% hydrate saturation showed no gas release at the seabed across all values of permeability. At low concentrations of hydrate, the amount of gas released on dissociation is very small and so the relative permeability for gas flow remains very low and gas movement through the sediments is slow. This is sensitive to the irreducible gas saturation parameter; increasing the value from 1 to 5% increases the delay significantly, as the volume of gas required to be produced before gas can flow increases (Figure 6d). The shortest delays are seen in low porosity, high permeability simulations. At the continuum scale, fractured sediment in which flow is

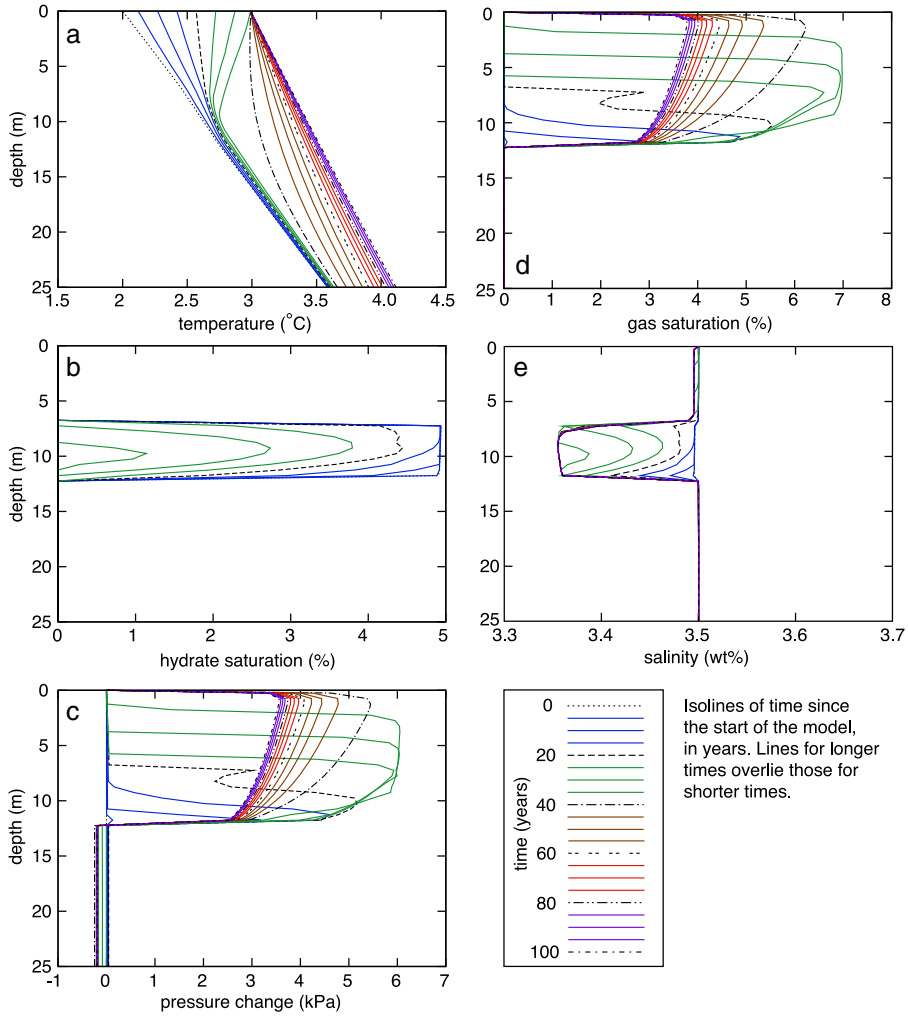


**Figure 5.** Results from model of hydrate dissociation as the seabed temperature at 390 m depth warms linearly from 2 to 3°C over a period of 33 years and then remains constant at 3°C until 100 years. The permeability used for the initial model is $10^{-13}$ m$^2$. Default values of the parameters are: initial depth to top of hydrate 7 m, porosity 60%, hydrate saturation 5%, irreducible gas saturation 2%. Pressure change (c) is the deviation from hydrostatic pressure.

concentrated in the fractures behaves as a low porosity, high permeability medium. With exception of the irreducible gas saturation, the default values of the parameters for the model, as used for the results displayed in Figure 5, yield the greatest lag times for a given permeability.

[16] The maximum rates of flow of methane into the ocean, for the same models illustrated in Figure 6, show a strong dependence on permeability, dropping off greatly for values of permeability less than $10^{-13}$ m$^2$ (Figure 7). This is, in part, the effect of raised pressure from the released gas in a low permeability medium increasing the stability of the hydrate and reducing the rate of dissociation. For a permeability of $10^{-17}$ m$^2$, typical of a glacial till, it takes longer than 100 years for the hydrate dissociate completely, whereas for a permeability of $10^{-13}$ m$^2$ it takes about 37 years (Figure 5c). Also, the gas has a low relative permeability, because gas saturation is low and as permeability decreases the increase in gas saturation is insufficient to increase the relative permeability of the gas to compensate for the decrease in absolute permeability. Increased depth to the top of the hydrate decreases the flow rate, because the excess pressure gradient is decreased by the increase in distance between the seabed and the dissociating hydrate. There is little sensitivity to variation in hydrate saturation above 10%.

[17] There is an upper limit to the maximum flow rate of around 1500 g·m$^{-2}$ yr$^{-1}$ across all the model runs. This limit is imposed by the rate of heat input. Once at the temperature for dissociation, hydrate requires an additional 55 kJ of energy to release one mole of methane. Limiting factors for the rate of heat input are the thermal diffusivity of the sediment and the rate of increase of the temperature of the seabed, which increases the thermal gradient. The importance of enthalpy in limiting the rate of dissociation of hydrate is demonstrated by how the rate of flow of gas from the seabed varies with time for different saturations of hydrate and rates of temperature increase at the seabed (Figure 8). Doubling the rate of temperature increase at the seabed from 0.03°·yr$^{-1}$ to 0.06°·yr$^{-1}$ cuts the delay for a model with hydrate saturation of 5% at a depth of 7 m by about 10 years, from 39 to 29 years and more than doubles the maximum flow rate. The rate at

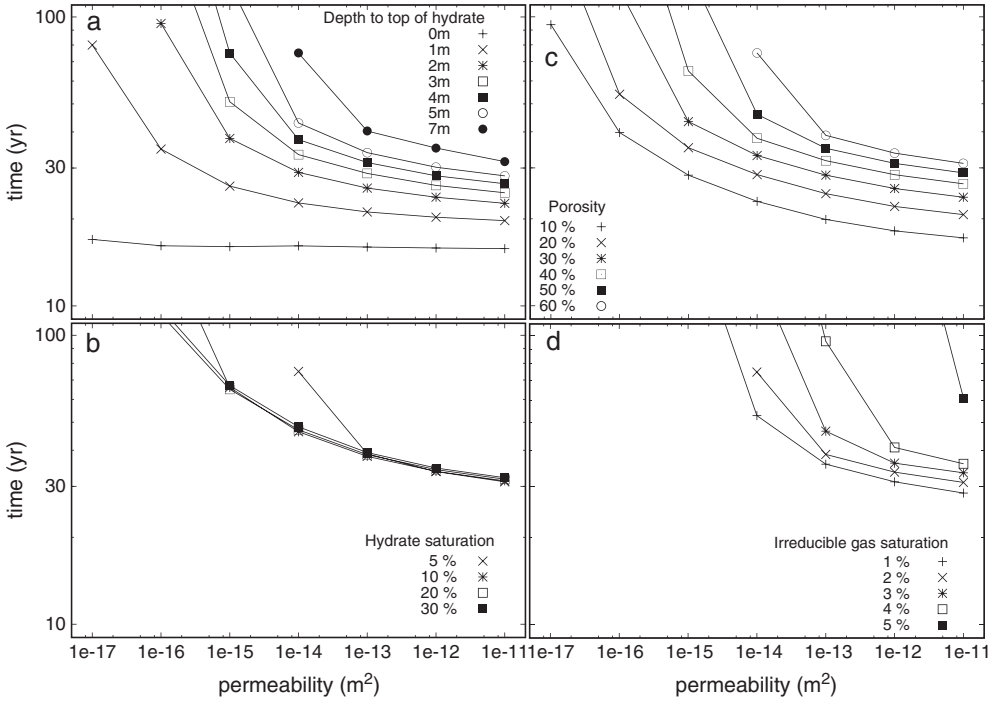


**Figure 6.** Time for methane to reach the seabed vs permeability for (a) initial depths to top of hydrate between 0 and 7 m; (b) hydrate saturations between 5 and 30 %; and (c) sediment porosity between 10 and 60 %. Initial hydrate saturation is 30, 15, 10, 7.5, 6 and 5% for porosity 10, 20, 30, 40, 50 and 60%, respectively; (d) irreducible gas saturate between 0.01 and 0.05. Default values of the parameters are: initial depth to top of hydrate 7 m, porosity 60%, hydrate saturation 5%, irreducible gas saturation 2%.

which the peak flow tails off depends on hydrate saturation. A greater degree of hydrate saturation produces a larger amount of gas, but its emission from the seabed is spread over a longer period. The onset of a period of methane gas expulsion is preceded, about half a year earlier, by a period of expulsion of methane-enriched water that has been displaced by the gas, which lasts about two years.

[18] Recent measurements (Feseker, personal communication, 2011) indicate that thermal conductivity is in the range 1.8–2.1 $W \cdot m^{-1}K^{-1}$, rather than the value of 1.21 $W \cdot m^{-1}K^{-1}$ used generally for the model, in the top few meters of sediment in the area in which the plumes occur and that thermal conductivity increases systematically as water depth decreases over the range 450–350 m, which is consistent with an increase in the proportion of rock fragments in the sediment and a decrease of porosity. The *Budiansky* [1970] model would suggest a porosity of 30% for sediment with a thermal conductivity of 1.8 $W \cdot m^{-1}K^{-1}$. Low porosity is expected in glacigenic deposits, because of their very poor sorting, which results in the smaller grains filling the pore spaces between the larger grains. Lower porosity for the shallow glacigenic sediment is consistent with the relatively high values of seismic velocity measured in these sediments [*Chabert et al.*, 2011]. The average velocity of about 1710 $m \cdot s^{-1}$ for the top 60 m of sediment indicates that the average porosity could be about 30%, although, without knowledge of clay content, one cannot exclude a porosity of between 25 and 35% or lower [*Kirsch*, 2006]. Assuming that heat flow is constant across the margin from where the BSR is present, 8 km farther downslope from the plume site, increased thermal conductivity of 1.8 $W \cdot m^{-1}K^{-1}$ throughout the sediment beneath the seabed would result in a thermal gradient of $44°C \cdot km^{-1}$ and the base of the hydrate stability zone would be deeper, at 35 m. The effect of the higher thermal conductivity and lower porosity on the emission of gas at the seabed is to speed up the first emergence of gas by 5 years. The depth of hydrate also plays a role in controlling the thermal gradient, as the temperature is tied to the dissociation temperature during hydrate dissociation. Shallower hydrate produces a steeper gradient and more rapid heat transfer.

### 3.2. Time Scales of Temperature Variation

#### 3.2.1. 1975–2008

[19] To examine whether the linear increase in the temperature at the seabed used to test the sensitivity of the model gave results that were different in any significant way from those from a model that was driven by the interannual near-bottom water-temperature data from the area of the Svalbard plumes over the period 1975–2008 [*Westbrook et al.*, 2009] (Figure 9), we ran a model with the same properties as the model discussed above (Figure 5), but with the seabed temperature varying as the recorded temperature for each year (1975–2008 series). For both models the seabed temperature remains constant at 3°C after 33 years. The results show that in all major respects the model with the linear increase in temperature provides an adequate representation of the response of the system (Figure 10). Gas first comes to the seabed at 34 years in the linear model and at about 36 years in the 1975–2008 series model (Figure 10d). During the period 20–25 years from the start of the run (1995–2000), new hydrate forms from gas released from earlier hydrate dissociation between 3.5 and 10 m in the 1975–2008 model. Hydrate disappears completely

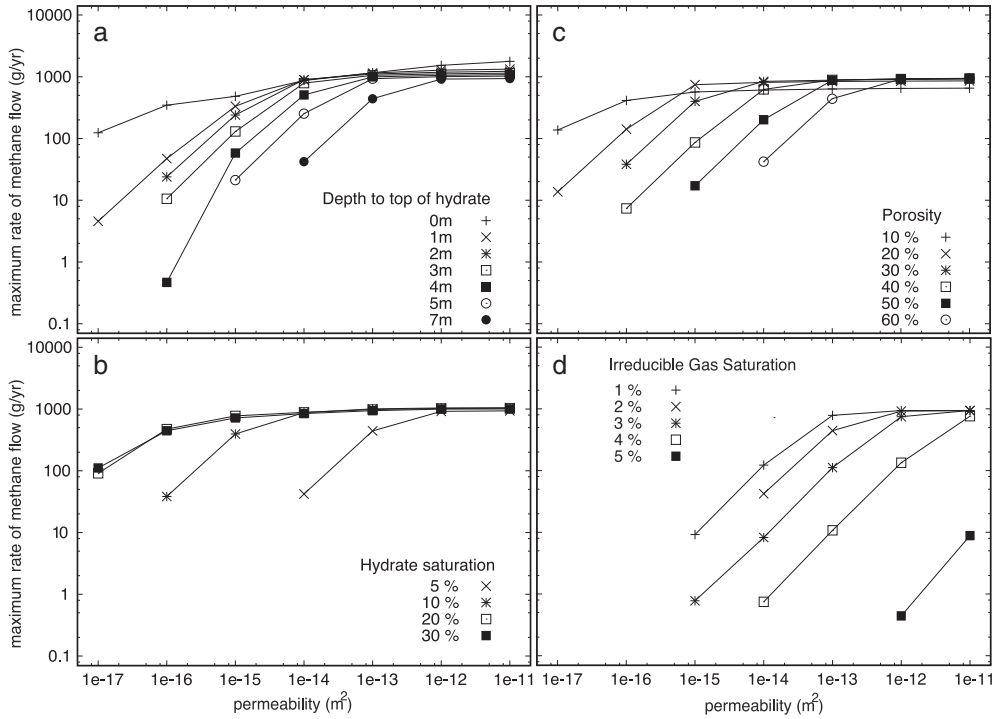


**Figure 7.** Maximum rate of methane release into the ocean vs permeability for (a) initial depths to top of hydrate between 0 and 7 m; (b) initial hydrate saturations between 5 and 30%; and (c) sediment porosity between 10 and 60%. Initial hydrate saturation is 30, 15, 10, 7.5, 6 and 5% for porosity 10, 20, 30, 40, 50 and 60% respectively; (d) irreducible gas saturation between 0.01 and 0.05.

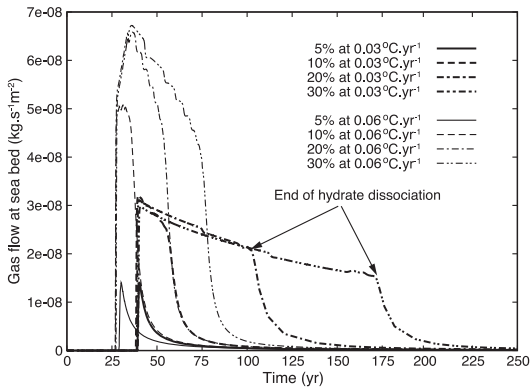


**Figure 8.** Flow of gas from the seabed as a function of time after the onset of warming. Initial hydrate saturation ranges from 5 to 30% and warming is at 0.03°C·yr$^{-1}$ and 0.06°C·yr$^{-1}$ over a period of 33 years after which the temperature is held constant.

2 years later in the 1975–2008 series model than in the linear model. The large fluctuations in the geotherm in the top 5 m do not penetrate below the hydrate, because the temperature is buffered by the enthalpy of the dissociation of hydrate.

### 3.2.2. Annual Temperature Variation

[20] The effects of annual temperature variation upon shallow hydrate, only a meter beneath the seabed, were investigated in a model at 420 m water depth, initialized with a bottom water temperature of 3.0°C on the top boundary, with a sinusoidal temperature change of 0.5°C about this value. The model setup is such that at steady state, hydrate is stable at the mean temperature of 3.0°C but not at the maximum temperature of 3.5°C. The initial model has hydrate from the BHSZ to 1 m below the seabed at 5% saturation. The model was run with 15 years of annual cyclical temperature variations and results from the 10th year are presented in Figure 11. The annual variation in temperature has little effect on the distribution of hydrate even in this model, close to the edge of the hydrate stability zone. Hydrate starts to dissociate when the temperature reaches its dissociation temperature, but because the process of dissociation is endothermic, the temperature in the sediment while hydrate is present is held at the hydrate dissociation temperature. This can be seen in Figure 11a, where temperature curves for times between 120 and 240 days lie close together where hydrate is present. Only a small amount of dissociation occurs before the temperature falls again and hydrate reforms from the gas produced during dissociation, which has not escaped to the seabed, because the level of gas saturation only exceeds the critical level required for it to be able to flow for about 80 days, and for that period the relative permeability of gas is so low that hardly any migration of gas occurs. Consequently, the annual variation in seabed temperature has little long-term effect on methane migration to the seabed from dissociation of hydrate beneath the seabed.

### 3.2.3. 1700–2008

[21] Earlier periods of warming may have predisposed the subseabed hydrate system to respond more quickly than predicted by a model with an invariant temperature field, in steady state, prior to the start of the model. In fact, it is certainly the case that the temperature conditions were

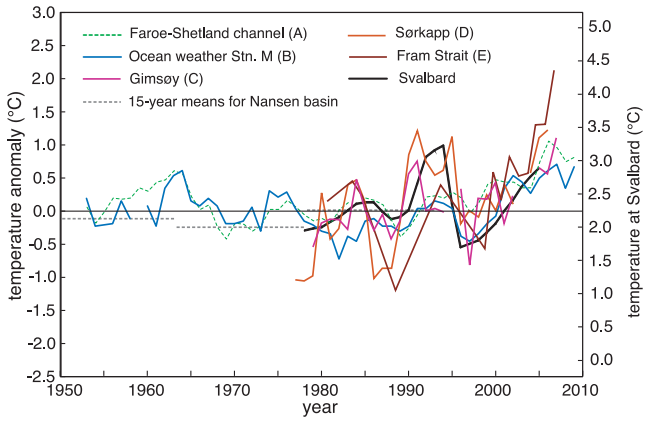


**Figure 9.** Water temperature data from stations and transects in the North Atlantic, A, B, C, D, E (Figure 1) [*Holliday et al*., 2008], near-bottom temperature data from the plume area off Svalbard [*Westbrook et al*., 2009] and 15 year mean values from the Nansen basin (Region 4 of *Polyakov et al*., 2004). The series A, B, C, D, E is plotted relative to the mean temperature calculated at each location over the time period 1978–2006 for all but the Faroe-Shetland Channel and Fram Strait, for which the time period 1988–2006 was used.

constantly changing. To discover how this would affect the results, we modeled the effect of temperature variations extending over centuries.

[22] To examine whether warming before 1975 contributed to hydrate dissociation, an evaluation was made of oceanographic data in the northeast Atlantic from the early 1950s until 2008. Temperature records from *Holliday et al*. [2008] at stations and transects shown in Figure 1 show very similar time variation along the pathway of Atlantic water flowing into the Arctic, and for the period after 1975 they show a similar time variation to the measurements from offshore Svalbard. However, there is a lag of about 3 years between Svalbard and the more southern stations, and the amplitude of variation at Svalbard is less strong for the near-bottom water in the range 350–400 m water depth. This behavior of pulses of warmer water of several years duration travelling into the Arctic has been recognized by others [e.g., *Walczowski and Piechura*, 2007]. The 30 years of data from offshore Svalbard since 1975 show a general warming trend from 1979 onward. Prior to this, however, the temperature records from other oceanographic stations and transects in the northeast Atlantic show cooling from a temperature maximum in the 1960s to a minimum around 1980 (Figure 9). Consequently, the period of most recent warming is no longer than about 30 years, much shorter than that needed by the model of *Reagan and Moridis* [2009], in which warming at a rate of 0.03°C per year for 100 years produces the first gas emission from the seabed after nearly 80 years of warming, which is consistent with the low permeability ($10^{-15}$ m$^2$) and low hydrate saturation (3% of pore space) used in their model, as demonstrated above.

[23] The ocean temperature record from 1950 to the present day is quite short in relation to the time scales of hydrate dissociation and gas migration and is made complicated by decadal variation [e.g., *Biastoch et al*., 2011]. Therefore, we investigated the possibility of extending the temperature record back to 1700. To construct a seabed temperature series (1700–2008A) to model the period

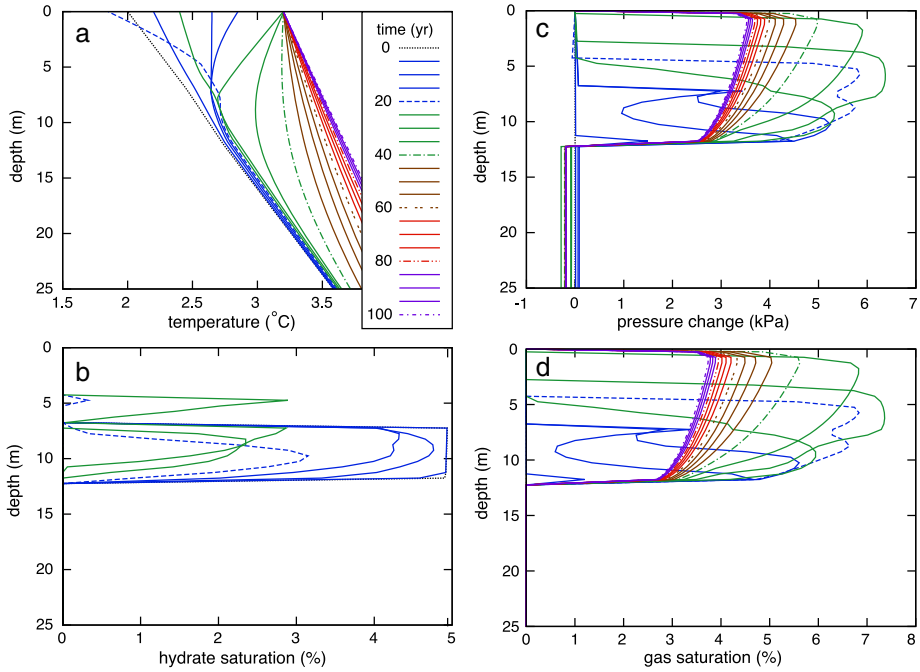


**Figure 10.** Results from model of hydrate dissociation as the seabed temperature at 390 m depth changes temperature according to the measured values from *Westbrook et al*. [2009] over 33 years (1975–2008 series), followed by constant temperature until 100 years. Time zero corresponds to 1975. All other parameters are identical to those for the model a linear increase in temperature illustrated in Figure 5.

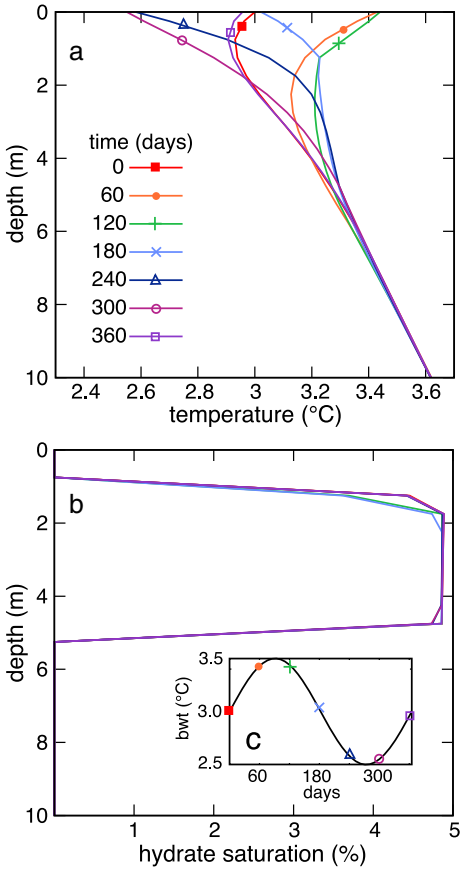


**Figure 11.** Effect of annual variation in bottom-water temperature on shallow hydrate at 1 m below the seabed in 420 m water depth. (Model properties the same as those for the model illustrated in Figure 5.) (a) Temperature profile every 30 days; (b) hydrate distribution every 30 days; and (c) bottom water temperature variation over 1 year.

1700–2008, we used the near-seabed temperature values of *Westbrook et al*. [2009] for 1975–2008, the values from *Holliday et al*. [2008] for 1950–1975, after scaling to those of *Westbrook et al*. [2009] to give near-seabed temperatures, and the15 year mean values of temperature from *Polyakov et al*. [2004] for the period 1900–1950, after scaling by matching the 15 year means of *Polyakov et al.* since 1950 to the temperature records from the Svalbard-Fram Strait area shown in *Holliday et al*. [2008] and *Westbrook et al*. [2009]. For the period 1700–1900, we used 50 year means taken from record of summer temperatures at 50 m water depth from *Spielhagen et al*. [2011], after scaling to values likely to represent the temperature at a depth 400 m by multiplying by a factor of 0.67, which is the ratio of interdecadal variation of temperature between the depth ranges 50–200 m and 416–793 m, obtained by *Biastoch et al*., [2011]. The baseline to which the scaled temperature values were tied was 2.25°C, the mean value of temperature measured at 400 m depth off Svalbard between 1978 and 2005 (Figure 12). There is a large degree of uncertainty in reconstructing the near-bottom temperature record for the period up until the latter part of the 20th century. Therefore, to examine the effect of uncertainty, we also modeled the effect of a temperature series (1700–2008B), for which the amplitude of variation, up to 1975, was half that used for 1700–2008A.

[24] Although the magnitude of increase of temperature is greatest for series 1700–2008A, the model, in which the top of the zone containing hydrate is at a depth of 7 m, predicts no emission of gas from the seabed, whereas gas emission from about 2005 onward is predicted for series 1700–2008B, which is a few years earlier than predicted by the model illustrated in Figure 10, which has the same properties but assumes a steady state situation at the beginning of the run of the model, in 1975. For both the models starting in 1700, a considerable quantity of hydrate remains in 2010, much more for series A than for series B, whereas the hydrate in the 1975–2008 model starting in 1975 disappears by 2010. This is a consequence of the enthalpy of hydrate dissociation. Insufficient heat has diffused into the zone containing hydrate to dissociate all the hydrate present. The greater depth of the base of the MHSZ, caused by the cooler initial temperature of series 1700–2008A, produces a thicker zone containing hydrate that takes a longer time to deplete. Dissociation is concentrated at the base of the hydrate. For 1700–2008B, with a thinner MHSZ and a smaller initial quantity of hydrate, the process of dissociation has progressed further in the upper part of the zone containing hydrate and gas released has migrated upward, reforming hydrate and subsequently being released again four times since 1950.

#### 3.2.4. 950–1950

[25] The starting models for 1700–2008A and B represent a steady state situation at 1700, but there were changes in ocean temperature before then. There was a major period of climate warming, the Medieval Warm Period between about 950 and 1250 A.D., and a period of cooling, the Little Ice Age between the mid-15th and mid-19th centuries. These show, respectively, relative warming of about 0.5°C and cooling by as much as –1°C west of Svalbard, relative to temperature in the early 20th century [*Spielhagen et al*., 2011], and more generally in the northernmost Atlantic and the Arctic [*Mann et al*., 2009]. To provide a simple simulation of the possible effect of these long-term variations on hydrate growth and dissociation, we ran a model over a 1000 year period between 950 and 1950 AD, in which we represented the variation in bottom-water temperature by a sine wave of 1°C amplitude with a maximum in 1200 A.D. and a minimum in 1700 A.D. For this model, rather than assume the extent of the zone invaded by hydrate and the degree of saturation, we included a source of methane gas at the base of the model and transport of gas by molecular diffusion. In the models described above, transport of methane has been by gas flow and advection of dissolved methane in water; transport by molecular diffusion was not included. Neither was it included in the models of *Reagan and Moridis* [2008, 2009]. While this simplification can be justified over short time periods, because the rate of diffusive transport is slow in comparison to gas flow and advection in solution, diffusion becomes important for time periods of hundreds of years or more, especially when hydrate is close to the seabed. Molecular diffusion with a diffusion coefficient of methane in water of $2\times10^{-9}$ m$^2$ s$^{-1}$ [*Lu et al*., 2006] is included in the 1000 year model. The model also has gas inflow from beneath, represented by a source of methane gas in the bottom cell of the model.

[26] The model was initialized with constant heat flow throughout and constant gas flow from the base of the model to the base of the hydrate stability field. Initially, there was

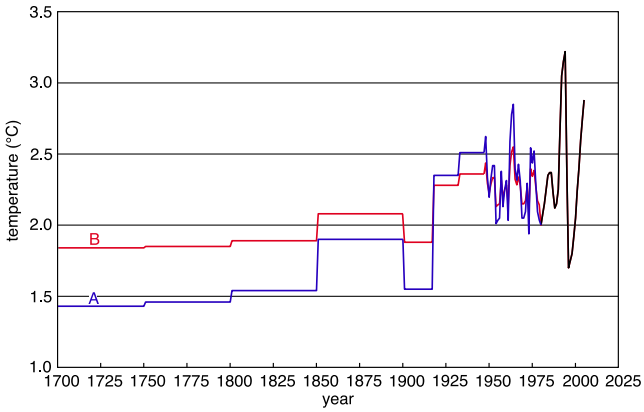


**Figure 12.** Temperature series used to model the effect of variation in seabed temperature on the subseabed hydrate and gas over the period 1700–2008. Both series finish with the annual values of near-seabed temperatures measured in the area from 1975–2008 (shown in black) [*Westbrook et al*., 2009]. For series 1700–2008A (blue), annual values for 1950–1975 were derived from *Holliday et al*. [2008], 15 year mean values for 1900–1950 from *Polyakov et al*. [2004] and 50 year mean values for 1700–1900 from *Spielhagen et al*. [2011]. The effect of the uncertainty in predicting the values of near-seabed temperature prior to 1975 was tested with series 1700–2008B (red), for which the deviation from the mean temperature of 2.25°C for years 1975–2005 is 50% of that of series 1700–2008A for the period up to 1975.

5% hydrate saturation from the base of the hydrate stability zone to 1 m below the seabed, in water depth of 390 m and with bottom water temperature of 2°C. The amount of gas input to the base of the model was varied between different runs of the model to determine those values that would sustain hydrate at a shallow depth beneath the seabed. The hydrate was initially 13 m thick, but it dissociated as temperature increased to 3°C, during warming of the seabed in the early part of the 1000 year period (Figure 14). As the seabed cooled, hydrate formed again, initially at the seabed and then deeper. Hydrate very close to the seabed was depleted by diffusion of methane into the seawater and the top of the hydrate dropped by 1.5 m over 500 years. As the base of the hydrate deepened, a zone developed in which both hydrate and gas were present, made possible by increased salinity caused by hydrate formation. By the end of the 1000 year period, hydrate and gas coexisted in the MHSZ, in all but the top 1 m of the model. A similar effect was exhibited by the models of *Liu and Flemings* [2007] to explain gas venting through the hydrate stability zone. The model presented here shows that hydrate can be maintained close to the seabed if gas inflow of a few tens of $mol \cdot m^{-2}\ yr^{-1}$ is present. With a gas inflow of 30 $mol \cdot m^{-2}\ yr^{-1}$, hydrate is sustained at a depth of 1.5 m (Figure 14). We do not claim that this model represents the actual variation in a hydrate concentration over the 1000 year period. The model, however, demonstrates that hydrate can be formed and sustained close to the seabed, even with loss of methane by diffusion to the seabed, if there is sufficient supply of methane from beneath the MHSZ. The model places the base of hydrate at a depth of 22 m after 800 years (equivalent to 1750 A.D.). For a similar excursion in temperature, the model for series 1700–2008A (Figure 13) places it at 30 m for 1750. The difference is largely a consequence of the preceding warm period up to 1450, whereas the starting model for 1700–2008A assumes thermal steady state at 1700. The shallow depth of hydrate, within 2 m of the seabed, from about 1550 onward, permits gas from dissociating hydrate to reach the seabed quickly during periods of substantial warming in the mid-to-late 20th century. This behavior is retained, even if the sediment has a low permeability of $10^{-15}$ $m^2$, as indicated by a model for 1700–2008A that takes as its initial value for the depth to the top of hydrate the depth of hydrate shown at 800 years by the 1000 year model (Figure 15).

## 4. Discussion

### 4.1. Sediment Hydraulic Properties

[27] Vertical migration of fluid through the glacigenic sediments (glacial diamictons) in the upper part of the sediment sequence will be impeded by their low intergranular permeability, which is likely to be around $10^{-17}$ $m^2$ [*Hubbard and Maltman*, 2000]. Yet the effective permeability required for the system to respond in the time frame of measured warming of the seabed (about 30 years) is about $10^{-13}$ $m^2$, 10,000 times higher. Consequently, it is very likely that fluid migration through the glacigenic sediments is primarily through cracks, which greatly increase the effective permeability of the sediment.

[28] The formation of cracks within the sediments at the top of the continental slope can be promoted by gravitationally induced downslope extensional stress. A large submarine slide immediately to the north of the principal area in which the plumes of methane bubbles exist, bears witness to the effect of gravitationally induced stress at this locality [*Vanneste et al*., 2007] and, farther downslope, *S*-wave anisotropy indicates the presence of aligned cracks in the shallow sediment [*Haacke et al*., 2009].

[29] The production of gas from hydrate increases pressure in sediment of low permeability, which will combine with the deviatoric tensional stress in the direction of the minimum principal stress to create cracks normal to the minimum principal stress. In the upper parts of models with a low permeability ($10^{-17}$ $m^2$ to $10^{-16}$ $m^2$) the pore pressure exceeds the lithostatic load only a few years after the dissociation of hydrate commences. Therefore, it is very unlikely that in reality very low permeability can be maintained when gas is being produced rapidly from hydrate dissociation. The gas does not have to invade all of the over-pressured section to do this, as pressure is transmitted through the pore water. Where cracks are the main conduits for flow, the flow paths have a high permeability but a small cross-sectional area, which results in a much higher flow velocity than for intergranular flow through sediment at the same flux rate. In weak sediment, fluid pressure does not need to achieve or exceed lithostatic pressure to open vertical fractures, because horizontal stress is normally less than the lithostatic vertical load. Observations during a natural hydrofracture event in shallow clay-rich sediments in the outer part of the Niger Delta showed pressure dissipation at a rate several orders of magnitude faster than would be expected if flow were through a pore network [*Sultan et al*., 2011]. Furthermore, numerical modeling of gas invasion in sediment [*Jain and Juanes*,

2009; *Holtzman and Juanes*, 2011] predicts that gas released by dissociating hydrate in fine-grained sediment of low permeability will migrate by propagating fractures.

[30] To simulate the expected behavior of a fractured clay layer with TOUGH+Hydrate, we set up a model in which the sediment above the base of the MHSZ has a very low porosity (1%) to represent the low volume of the fracture network. This approximation takes advantage of flow through the sediment matrix being so small in comparison to flow through the fractures that matrix flow can be ignored. The permeability is high ($10^{-12}$ m$^2$) and could be much higher in the real system, but is limited in the model to ensure model convergence. The reduction in the volume of the principal flow paths (i.e., the fractures instead of the pores) increases the flow rate inversely for a constant flux. Therefore, the flow rate through fractures occupying 1% of the sediment will be 60 times faster than flow through pores occupying 60% of the sediment. The fractures initially contain hydrate at 60% saturation, which is an equivalent volume of hydrate to 1% saturation in the models with 60% porosity. The presence of the fractured layer enables gas from dissociation of hydrate that is greater than 7 m below the seabed to reach the seabed about 18 years after the beginning of warming of the seabed and about 10 years after the hydrate begins to dissociate (Figure 16). By comparison, a model with permeability of $10^{-17}$ m$^2$ and porosity 60%, representing the matrix of the sediment, does not show any gas flow at the seabed, because the gas is trapped in the pore space and the build up of high pressure in an unfractured material of this low permeability increases hydrate stability, slowing its dissociation.

### 4.2. Evaluation of Model Results in Light of Observations of Gas Emissions and Subseabed Geology

[31] Gas flow is uniform in the model, but gas does not seep uniformly from the seabed in the region of the plumes of gas bubbles off Svalbard (Figure 2). Seepage occurs at specific sites in zones that are typically elongate, subparallel to the bathymetric contours, implying local stratigraphic control, such as the outcrops or subcrops of more permeable layers, or structural control, such as zones of cracks and faults, although no faults with large displacement have been recognized so far in the seismic reflection data. This pattern is superimposed upon that imposed by the landward limit of the MHSZ, which, itself, runs parallel to the bathymetric

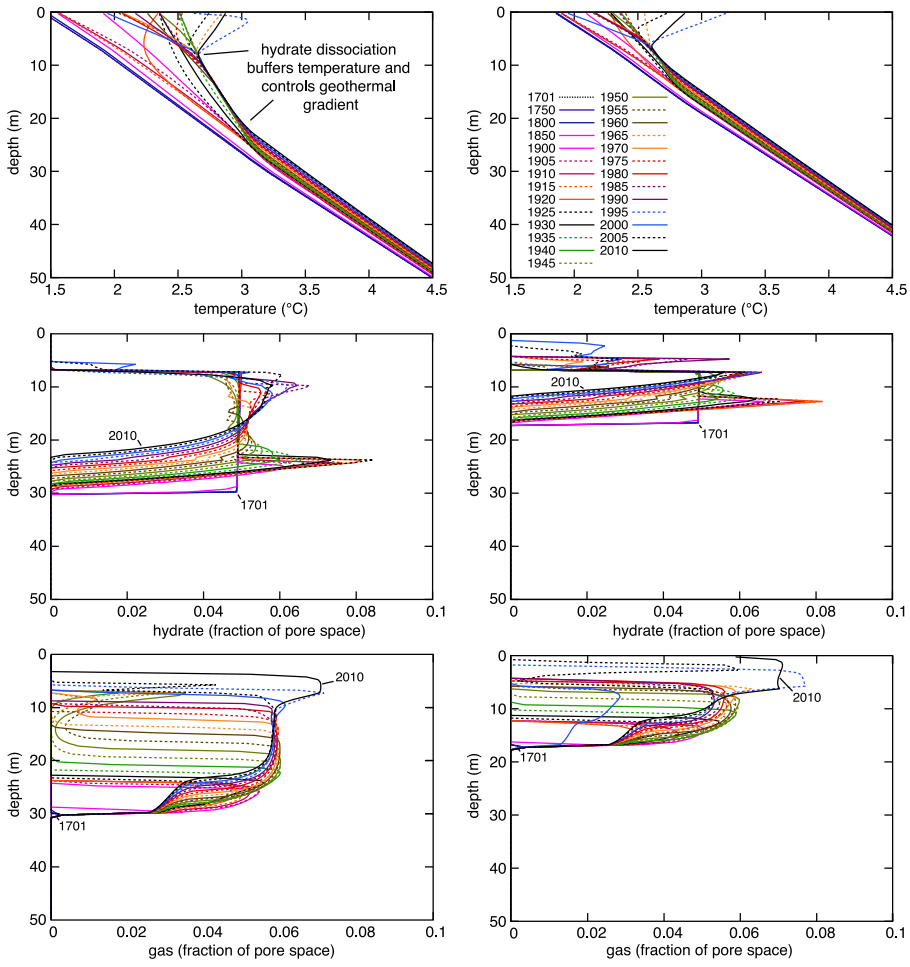


**Figure 13.** Results from model of hydrate dissociation as the seabed temperature at 390 m depth varies over the period 1700–2008 according to series 1700–2008A (left-hand column) and series 1700–2008B (right-hand column), shown in Figure 12. The parameters for the initial model are permeability $10^{-13}$ m$^2$, depth of top of hydrate 7 m, porosity 60%, hydrate saturation 5%, irreducible gas saturation 2%.

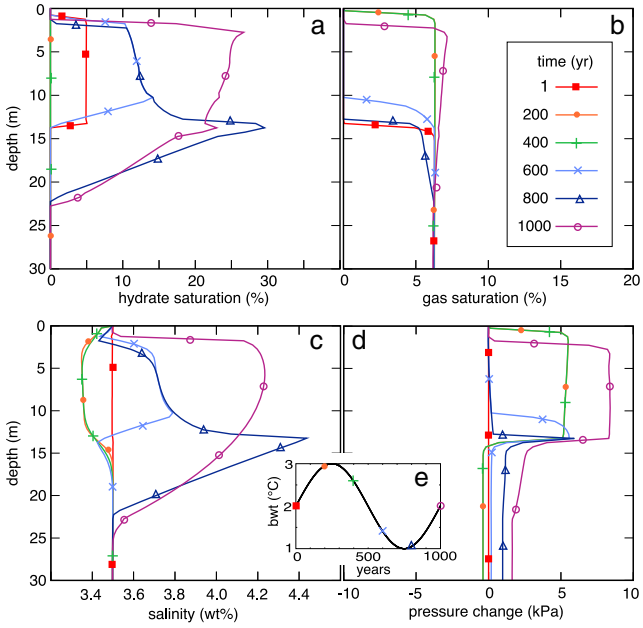


**Figure 14.** Simulated effect on the hydrate system of major periods of climate warming and cooling over the last 1000 years, represented by the sine curve shown inset (e). Model parameters are identical to those for Figure 5.

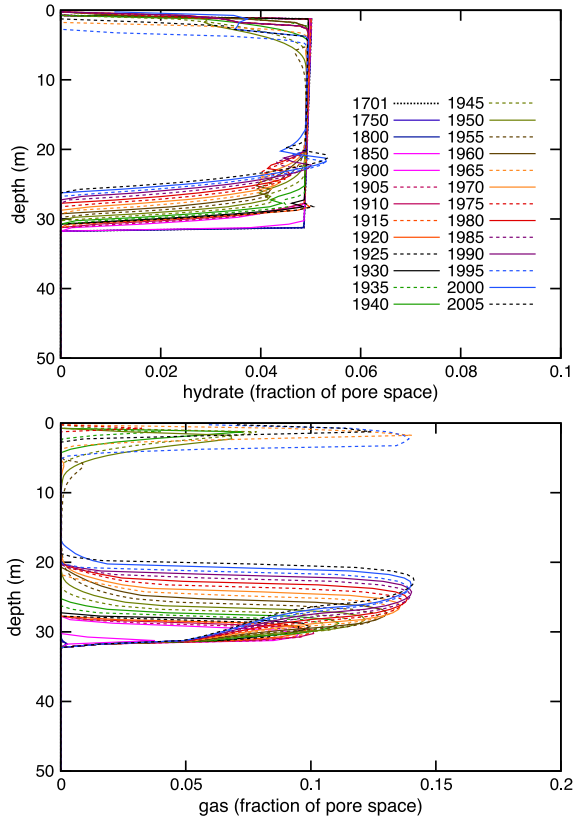


**Figure 15.** Results from model of hydrate dissociation, as the seabed temperature at 390 m depth varies over the period 1700–2008 according to series 1700–2008A, shown in Figure 12. The parameters for the initial model are permeability $10^{-15}$ m$^2$, depth of top of hydrate 1 m, porosity 60%, hydrate saturation 5%, and irreducible gas saturation 2%.

contours at about 400 m depth. It is very likely that this zonation of methane outflow owes as much to litho-stratigraphic control of the zones in which hydrate was formed, possibly from methane-saturated pore water in the more permeable sedimentary units, as it does to litho-stratigraphic channeling of methane gas released by dissociation of hydrate.

[32] The outflowing gas is already focused into trains of gas of locally high concentration before it reaches the seabed, probably exploiting a subseabed fracture network and lithological heterogeneity. The 1D approximation used in the models cannot represent the mechanisms by which this focusing occurs. Indeed, although existing seismic data show the heterogeneous nature of the stratigraphy and structure clearly [*Sarkar et al.*, 2011a; *Rajan et al.*, 2012; *Sarkar et al.*, 2012], there are far from sufficient data available to define the subsurface structure and properties well enough for meaningful 2D or three-dimensional modeling of the flow regime. We consider that the 1D models do, however, provide insights to understanding the response to a warming event that could be expected from a natural subseabed hydrate system, in terms of its overall thermal behavior and the budget of hydrate and methane release.

[33] The 1D models will overestimate the lag time between the start of warming and the appearance of gas at the seabed. In the real, three-dimensional system, lag times will be shorter. where hydrate is localized in the flow paths of methane migration, because their three-dimensional geometry presents a greater surface area to warming from the surrounding sediment and because gas can migrate laterally along higher permeability layers to join and reinforce established flow paths across the lower permeability layers. Gas joining preexisting flow paths will reach the seabed faster, because increasing the gas saturation in a flow path increases its relative permeability.

[34] With gas flow focused toward specific sites at the seabed, the flow of gas into the ocean is spatially very heterogeneous. Observations of the gas bubbles as they leave seeps in the seabed off Svalbard indicate quite a low rate of flow of gas [*Fisher et al.*, 2011]. Measurements of gas emission in other areas, such as South Hydrate Ridge, have recorded flux rates over 100 mol·m$^{-2}$ yr$^{-1}$ in close proximity to vents [*Heeschen et al.*, 2005], compared with regional averages of less than 2 mol·m$^{-2}$ yr$^{-1}$ [*Heeschen et al.*, 2005; *Artemov et al.*, 2007] at Hydrate Ridge and in the Black Sea. In the model presented here, hydrate is sustained very close to the seabed for rates of gas flux into its base of several tens of mol·m$^{-2}$ yr$^{-1}$ (Figure 14). These rates are likely to be typical of zones of focused gas flow.

[35] In the areas of plume occurrence close to the landward boundary of the MHSZ, plumes typically have a separation of 100 to 150 m. The smallest separation is about 35 m. Each plume, therefore, represents, on average, the free gas output of an area of roughly 15,000 m$^2$ and could be considered to be the product of processes in the subseabed volume beneath the plume that act to focus the outflow of gas at the seabed (Figure 17). Dividing the input flux of gas (30 mol·m$^{-2}$yr$^{-1}$) to the base of the 1000 year model (Figure 14) by 15,000, to compensate for the effect of focusing the outflow of gas, provides a rough estimate of the average gas influx of 2 mMol·m$^{-2}$yr$^{-1}$ to the area. This, however, provides only a likely lower bound on the flux, as we have insufficient information on the actual fluxes through the plumes, the flux of methane through the

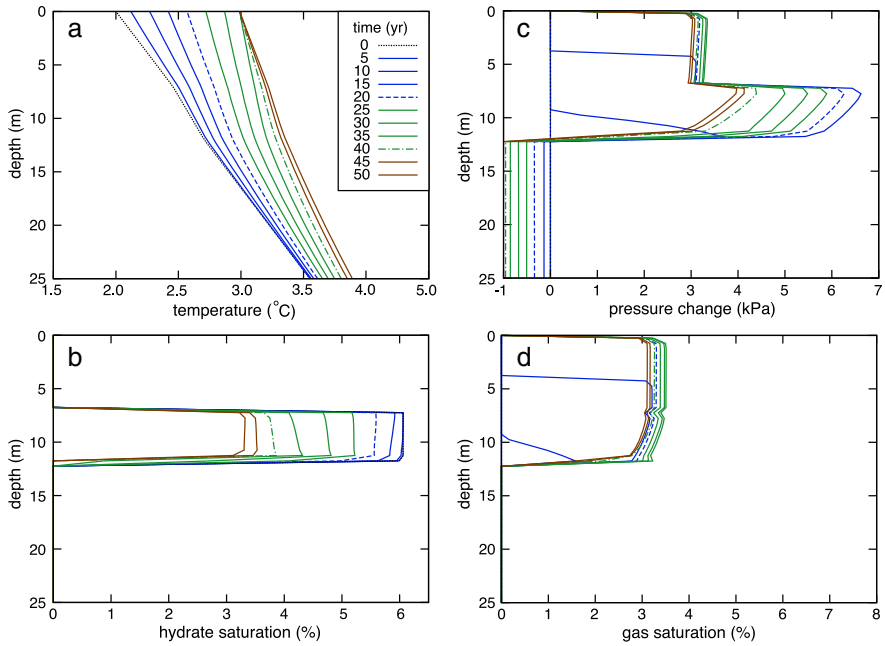


**Figure 16.** Results from a model of hydrate dissociation, in which sediment shallower than 14 m comprises a fractured layer with permeability $10^{-12}$ $m^2$ and porosity of 1%. The seabed temperature at 390 m depth warms linearly from 2 to 3°C over a period of 33 years and then remains constant at 3°C until 100 years. The properties and boundary conditions of the model are, otherwise, the same as those for the model displayed in Figure 5.

seabed by advection in aqueous solution and by molecular diffusion outside the close vicinity of the plumes occur to able to provide a more accurate estimate.

[36] Although the modeling has been carried out for a water depth of 390 m, in which the youngest gas plumes should be present, it should not be forgotten that the MHSZ withdrew earlier from beneath the seabed in shallower water, promoting the emission of gas plumes progressively farther downslope, as water temperature increased after the minimum of the Little Ice Age in the middle of the 17th century

**Table 2.** Summary of the Values of Variable Parameters for All the Runs of the Models Presented. Default Values of the Parameters are: Initial Depth to Top of Hydrate 7 m, Porosity 60%, Hydrate Saturation 5%, Irreducible Gas Saturation 2%, Permeability Used for the Initial Model (Excluding the Effect of Hydrate) $10^{-13}$ $m^2$

| Run | Values of Variable Parameters |
|---|---|
| Depth to top of hydrate time lag (Figure 6a); Max rate of methane release (Figure 7a) | Permeability: 1E-11, 1E-12, 1E-13, 1E-14, 1E-15, 1E-16, 1E-17 $m^2$<br>Depth to top of hydrate: 0,1,2,3,4,5,7 m |
| Porosity time lag (Figure 6b); Max rate of methane release (Figure 7b) | Permeability: 1E-11, 1E-12, 1E-13, 1E-14, 1E-15, 1E-16, 1E-17<br>Porosity: 10, 20, 30, 40, 50, 60% |
| Hydrate saturation time lag (Figure 6c); Max rate of methane release (Figure 7c) | Permeability: 1E-11, 1E-12, 1E-13, 1E-14, 1E-15, 1E-16, 1E-17<br>Hydrate saturation: 5, 10, 20, 30% |
| Irreducible gas saturation time lag (Figure 6d); Max rate of methane release (Figure 7d) | Permeability: 1E-11, 1E-12, 1E-13, 1E-14, 1E-15, 1E-16, 1E-17<br>$S_{irG}$: 1, 2, 3, 4, 5 % |
| Rate of gas flow from seabed (Figure 8) | Hydrate saturation: 5, 10, 20, 30%<br>Warming rate: 0.03, 0.06°C·$yr^{-1}$ |
| Temperature record 1975–2008 (Figure 10) | Recorded near-seabed temperatures, as displayed in Figure 9 |
| Annual cycle (Figure 11) | Ocean temperature varies daily, following a sinusoidal annual cycle between 2.5 and 3.5°C; top of hydrate is at 1 m. |
| 1700–2008 temperature series (Figures 13 and 15) | Driven by the variations in temperature shown as curves A and B in Figure 12. |
| 1000 years Represents, approximately, the Medieval Warm Period and the Little Ice Age (Figure 14) | Ocean temperature varies over 1000 years following a sine curve varying between 1°C and 3°C; top of hydrate initially at 1m; gas source of 30 mol·$m^2$ $year^{-1}$ at base of model; molecular diffusion is active. |
| Fracture flow (Figure 16) | Sediment shallower than 14 m has permeability $10^{-12}$ $m^2$ and porosity 1%. |

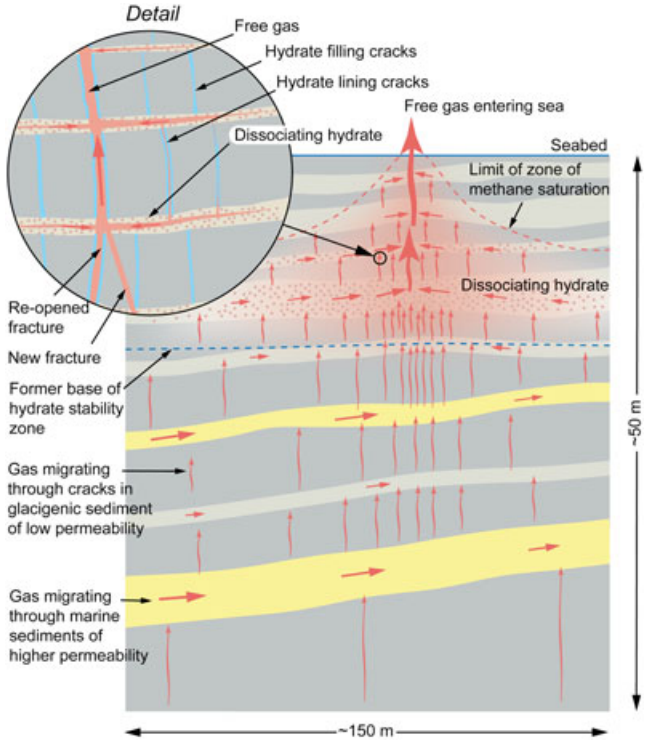


**Figure 17.** Speculative illustration of the processes and geological structure beneath a site of gas emission from the seabed, depicting how gas beneath the MHSZ and gas released from dissociating hydrate may be focused by fractures and entrainment into more vigorous flow paths. Primarily glacigenic sediment of low intrinsic permeability is shown in gray, with lighter tone having relatively higher permeability. Units of marine sediment with high permeability are shown in yellow. Focusing of the flow of free gas and methane-saturated water will have controlled where hydrate was most concentrated within the MHSZ, providing an already localized source of gas when the hydrate dissociates from the effect of warming. Overpressure generated by the production of gas from the zones of hydrate concentration could create or reopen fractures to increase permeability. The migration of gas will be focused further by its entrainment in the flow paths with the highest relative permeability in the opened fracture network.

[*Spielhagen et al.*, 2011]. Since 1800, when (from temperature series 1700–2008A) the seabed temperature was 1.5°C, the top of the MHSZ has deepened from 340 m water depth. Consequently, the western (deeper) boundary of the zone of emissions of gas from the seabed will have migrated downslope as the MHSZ retreated and was no longer present to capture methane migrating to the seabed by turning it to hydrate. The seabed in water shallower than 300 m has possibly not been underlain by hydrate since the last glacial period. Gas emitted from the seabed much shallower than 300 m is likely to have migrated through the underlying marine sequence without ever having been in hydrate. Gas emitted from the seabed in the depth range 360–250 m could come from hydrate dissociation or from the underlying marine sequence and have migrated along the westward-dipping strata that crop out at the seabed or beneath a thin glacial cover (Figure 3).

## 5. Conclusions

[37] Oceanographic data from the NE Atlantic indicate that, although complicated by decadal-scale variation, recent warming of the near-seabed water in the uppermost part the western continental margin of Svalbard started around the year 1980 and was preceded by a period of cooling from a high in the 1960s. These recent variations in temperature are part of a more general warming of more than 1°C between the beginning of the 19th century and the beginning of the 21st century. If the gas in the bubble plumes observed in 2008 comes from hydrate dissociation caused by recent warming, then the time between onset of warming and methane release at the seabed for the plumes from seeps in water depths of between 390 and 400 m should be less than about 30 years.

[38] The principal conditions that reduce the time lag between warming and the onset of gas flow at the seabed are: (a) high permeability sediment, (b) low porosity sediment, (c) hydrate at a shallow depth beneath the seabed, and (d) increased rate of seabed warming. This time lag can be less than 30 years in water depths a few meters shallower than the present upper limit of the methane hydrate stability zone, where, for example, the top of the hydrate at >5% saturation in sediment with porosity <50% and permeability $>10^{-13}$m$^2$ is initially <5 m below sea floor.

[39] Unless the top of the hydrate is initially very shallow, a meter or so beneath the seabed, the short time between the onset of warming and the appearance of gas at the seabed requires fractures (cracks) in the low-permeability glacial sediments to enhance flow. Indeed, the modeling demonstrates the necessity of the presence of fractures, because, for values of permeability less than $10^{-16}$ m$^2$, gas pressure builds up to lithostatic pressure in less than 30 years and would generate fractures. The flow properties of a fractured system, high permeability, and low porosity (low storage) enable gas to transit rapidly. Depending on the degree to which permeability is increased by fractures, gas produced from the dissociation of hydrate that was as deep as 7 m could be contributing to present-day gas emissions.

[40] The enthalpy of the hydrate dissociation reaction plays an important role in restricting the rate of production of gas from dissociation. For a given rate of warming, the concentration of hydrate, above a certain fraction of pore space, does not affect the rapidity of the response to warming or the peak rate of gas flow. When more hydrate than this limiting fraction is present in the sediment, the period for which the release of methane can be sustained is increased. In the examples that we modeled, the limiting fractions were nearly 10% for warming of 0.03°C/yr and about 20% for warming of 0.06°C/yr (Figure 8). The dissociation reaction buffers the temperature, which increases only gently in response to increases in pressure and salinity caused by the release of gas and pure water, which increase the stability of the remaining hydrate. The geothermal gradient is locally tied to that of hydrate stability curve until the hydrate has disappeared (Figures 5a, 10a, 13). The process acts as a heat sink and the more hydrate that is present the longer it takes for the subsurface to warm in response to increasing temperature at the seabed.

[41] The effect of large quantities of deep hydrate, as predicted by the models for 1700–2008 A and B is to delay the flow of gas to the seabed, because, in the initial stages, heat is primarily consumed by the dissociation of the deep

hydrate rather than the warming and dissociation of shallow hydrate. To reach the seabed the gas released from the base of the zone of hydrate would have to migrate around the MHSZ, which would still exist at the present day and contain hydrate, or be injected through the MHSZ in fractures opened by overpressure.

[42] Cycles of warming followed by cooling successively increase the concentration of hydrate at shallower depths, as gas released from hydrate migrates upward before forming hydrate again, which leads to earlier gas release with each successive cycle. From the results of the 1700–2008 B model, it seems likely that gas was emitted from the seabed at a depth of 390 m during the mid-1960s.

[43] Over periods of hundreds of years, a flux of methane gas of a few tens of mol/m$^2$/yr is needed to maintain hydrate close to the seabed against loss of methane by diffusion. This rate of supply of methane, however, is only required to sustain shallow hydrate in the close proximity of the gas plumes. The average flux of methane over a large region could be three orders of magnitude less, with heterogeneous, geologically controlled migration and flow-focusing providing a much higher level of input of methane to the base of the MHSZ beneath the plumes. The supply of gas from deeper in the system is evident in the continental margin of west Svalbard, where gas is migrating upslope from the deeper offshore part of the continental margin.

[44] While the underlying cause of gas escape from the seabed off Svalbard is the migration to the seabed of gas originating deeply within the underlying marine sediments, the MHSZ combined with the laterally variable stratigraphy of shallow glacigenic and glaciomarine sediments controls the geographic distribution of hydrate and gas seeps. This is, first, by controlling where hydrate is formed and, second, by controlling the routes taken by gas released from dissociation of hydrate, as well as gas from beneath the MHSZ, to migrate to the seabed. With decreasing water depth landward of the MHSZ, gas migrating beneath the MHSZ is likely to be increasingly important as the source of gas emitted from the seabed. In the region of 370–400 m water depth however some, at least, of the gas that is emitted from the seabed must have come from hydrate that occupied that region before warming commenced, as the presence of the MHSZ will have caused gas entering it from below to be turned to hydrate.

[45] We envisage that the release of methane from hydrate in the 370–400 m water depth range is only the most recent phase of a continual increase of area of seabed from which methane is released, as water temperatures increased since the last glacial period, inducing an oscillatory but progressive withdrawal of the MHSZ into deeper water. Given the evidence for abundant supply of gas migrating into the upper continental slope and shelf, it is very likely that gas emission from the seabed has occurred here since the Little Dryas. Although, at present, it appears that no gaseous methane reaches the sea surface [*Fisher et al*., 2011], we would expect to see shorter response times and greater peak-flow rates for gas released from hydrate, if warming were to accelerate in the future. It may then be possible for gas emissions to be strong enough for methane to reach the atmosphere, especially if gas were stored transiently in traps sealed by hydrate, from which the escape of gas would be rapid when breached.

[46] **Acknowledgments.** This work was supported by the Natural Environment Research Council as a part of its Arctic Initiative for the International Polar Year 2007–2008 (grant number NE/D005728). The captain and crew of RRS *James Clark Ross* provided essential support for the acquisition of the data during research cruise JR211. We thank Matt Reagan and George Moridis for their advice and assistance with the use of the TOUGH+Hydrate modeling software and for providing an early release of their new diffusion code for the software in 2010. Thomas Feseker generously provided early results from his heat-flow measurements made in 2009. Our colleagues, Christian Berndt, Anne Chabert and Rachael James, gave encouragement and practical support through discussion and their work on other aspects of the investigation of gas release from the margin of west Svalbard.

## References

Archer, D., B. Buffett and V. Brovkin (2009), Ocean methane hydrate as a slow tipping point in the global carbon cycle, *Proceedings of the National Academy of Science USA*, *106*, 20596-20601, doi:10.1073/pnas.0800885106.

Artemov, Y., V. N. Egorov, G. G. Polikarpov, and S. B. Gulin (2007), Methane emission to the hydro- and atmosphere by gas bubble streams in the Dnieper Paleo-Delta, Black Sea, *Marine Ecological Journal*, *3*, (6), 3-25.

Biastoch, A., T. Treude, L. H. Rupke, U. Riebesell, C. Roth, E. B. Burwicz, W. Park, M. Latif, C. W. Böning, G. Madec, and K. Wallmann (2011), Rising Arctic Ocean temperatures cause gas hydrate destabilization and ocean acidification, *Geophysical Research Letters*, *38*, L08602, doi:10.1029/2011GL047222.

Budiansky, B. (1970), Thermal and thermoelastic properties of isotropic composites, *Journal of composite Materials*, *4*, 286-295.

Chabert, A., T. A. Minshull, G. K. Westbrook, C. Berndt, K. E. Thatcher, S. Sarkar (2011), Seismic characterisation of gas hydrate and free gas along the western continental margin of Svalbard, *Journal of Geophysical Research*, *116*, B12102, doi:10.1029/2011JB008211.

Dickens, G. R., J. R. O'Neal, D. K. Rea, and R. M. Owen (1995), Dissociation of oceanic methane hydrate as a cause of the carbon isotope excursion at the end of the Paleocene, *Paleoceanography*, *10*, 965-971, doi:10.1029/95PA02087.

Dmitrenko, I. A., S. A. Kirillov, L. B. Tremblay, H. Kassens, O. A. Anisimov, S. A. Lavrov, S. O. Razumov, and M. N. Grigoriev (2011), Recent changes in shelf hydrography in the Siberian Arctic: Potential for subsea permafrost instability, *J. Geophys. Res.*, *116*, C10027, doi:10.1029/2011JC007218.

Driscoll, N.W., J.K. Weissel, J.A. Goff, (2000), Potential for large-scale submarine slope failure and tsunami generation along the US mid-Atlantic coast, *Geology*, *28*, (5), 407-410 DOI: 10.1130/0091-7613(2000)28<407:PFLSSF>2.0.CO;2

Fisher, R.E., S. Sriskantharajah, D. Lowry, M. Lanoisellé, C. M. R. Fowler, R. H. James, O. Hermansen, C. Lund Myhre, A. Stohl, J. Greinert, P. B. R. Nisbet-Jones, J. Mienert, and E. G. Nisbet, (2011), Arctic methane sources: Isotopic evidence for atmospheric inputs, *Geophysical Research Letters*, *38*, L21803, doi:10.1029/2011GL049319.

Forster, P., V. Ramaswamy, P. Artaxo, T. Berntsen, R. Betts, D. W. Fahey, J. Haywood, J. Lean, D. C. Lowe, G. Myhre, J. Nganga, R. Prinn, G. Raga, M. Schulz, and R. Van Dorland (2007): Changes in Atmospheric Constituents and in Radiative Forcing. In: Climate Change 2007: the physical science basis. Contribution of Working Group I to the Fourth Assessment Report of the Intergovernmental Panel on Climate Change [Solomon S., D. Qin, M. Manning, Z. Chen, M. Marquis, K. B. Averyt, M. Tignor and H. L. Miller (eds.)]. Cambridge University Press, Cambridge, United Kingdom and New York, MY, USA.

Haacke, R.R. and Westbrook, G.K. (2006), A fast and robust method for detecting and characterising azimuthal anisotropy with marine *PS* converted waves, and its application to the continental slope of west Svalbard, *Geophysical Journal International*, *167*, 1402-1412, doi:10.1111/j.1365-246X.2006.03186.x

Haacke, R. R., G. K. Westbrook and S. Peacock, (2009), Layer stripping of shear-wave splitting in marine PS-waves: an investigation into the practical limits of resolution, *Geophysical Journal International*, *176*, 782-804, doi: 10.1111/j.1365-246X.2008.04060.x

Hassol, S. J. (2004), Impacts of a warming Arctic - Arctic climate impact assessment. Cambridge University Press, Cambridge.

Heeschen, K. U., R. W. Collier, M. A. de Angelis, E. Suess, G. Rehder, P. Linke, and G. P. Klinkhammer (2005), Methane sources, distributions, and fluxes from cold vent sites at Hydrate Ridge, Cascadia Margin, *Global Biogeochemical Cycles*, *19*, GB2016, doi:10.1029/2004GB002266.

Holliday, N. P., S. L. Hughes, S. Bacon, A. Beszczynska-Möller, B. Hansen, A. LavÍn, H. Loeng, K. A. Mork, S. Østerhus, T. Sherwin, and W. Walczowski (2008), Reversal of the 1960s to 1990s freshening trend in the northeast North Atlantic and Nordic Seas, *Geophysical Research Letters*, *35*, L03614, doi:10.1029/2007GL032675.

Holtzman, R., and R. Juanes (2011), Thermodynamic and hydrodynamic constraints on overpressure caused by hydrate dissociation: A pore-scale model, *Geophysical Research Letters*, *38*, L14308, doi:10.1029/2011GL047937.

Hubbard, B., and A. Maltman, (2000) Laboratory investigations of the strength, static hydraulic conductivity and dynamic hydraulic conductivity of glacial sediments, *Geological Society, London, Special Publications*, *176*, 231-242, doi: 10.1144/GSL.SP.2000.176.01.18.

Jain, A. K., and R. Juanes, (2009), Preferential mode of gas invasion in sediments: Grain-scale mechanistic model of coupled multiphase fluid flow and sediment mechanics, *Journal of Geophysical Research*, *114*, B08101, doi: 10.1029/2008JB006002.

Kennett, J., K. G. Cannariato, I. L. Hendy, and R. J. Behl (2003), Methane hydrates in quaternary climate change: the clathrate gun hypothesis, p. 216. Washington, DC: American Geophysical Union.

Kirsch, R., (2006), Petrophysical properties of permeable and low-permeable rocks, in R. Kirsch (ed.), Groundwater Geophysics (2nd ed.), Springer Berlin Heidelberg, 548pp., SN - 978-3-540-29387-3, 10.1007/3-540-29387-6_1.

Landvik, J. Y., O. Ingolfsson, J. Mienert, S. J. Lehman, A. Solheim, A. Elverhøi, and D. Ottesen (2005), Rethinking LateWeichselian ice-sheet dynamics in coastal NW Svalbard, *Boreas*, *34*, 7 – 24, doi:10.1080/03009480510012809.

Liu, X., and P. B. Flemings (2007), Dynamic multiphase flow model of hydrate formation in marine sediments, *Journal of Geophysical Research*, *112*, B03101, doi:10.1029/2005JB004227.

Lu, W. J., I. M. Choi, R. C. Burruss, and M. Z. Yang (2006), In Situ study of mass transfer in aqueous solutions under high pressures via Raman Spectroscopy: A new method for the determination of diffusion coefficients of methane in water near hydrate formation conditions, *Applied Spectroscopy*, *60*, (2), 122-129.

Mann, M. E., Z. Zhang, S. Rutherford, R. S. Bradley, M. K. Hughes, D. Shindell, C. Ammann, G. Faluvegi, and F. Ni (2009), Global Signatures and Dynamical Origins of the Little Ice Age and Medieval Climate Anomaly, *Science*, *236*, 1256-1260, 10.1126/science.1177303.

Micallef, A., C. Berndt, D.G. Masson, D.A.V. Stow, (2008), Scale invariant characteristics of the Storegga Slide and implications for large-scale submarine mass movements, *Marine Geology 247*, 46–60.

Moridis, G. J. (2003), Numerical studies of gas production from methane hydrates, *SPE J.*, *32*, 359-370.

Moridis, G. J., M. B. Kowalsky, and K. Pruess (2008), TOUGH+HYDRATE v1.0 user's manual: A code for the simulation of system behaviour in hydrate-bearing geological medial, *Per. LBNL-0149E*, Lawrence Berkeley Natl. Lab., Berkeley, Calif.

Polyakov, I. V., G. V. Alekseev, L. A. Timokhov, U. S. Bhatt, R. L. Colony, H. L. Simmons, D. Walsh, J. E. Walsh, and V. F. Zakharov (2004), Variability of the Intermediate Atlantic Water of the Arctic Ocean over the Last 100 Years, *Journal of Climate*, *17*23, 4485-4497.

Rajan, A., J. Mienert, S. Bunz (2012), Acoustic evidence for a gas migration and release system in Arctic glaciated continental margins offshore NW-Svalbard, *Marine and Petroleum Geology*, *32*, 36-49.

Reagan, M. T., and G. J. Moridis (2008), Dynamic response of oceanic hydrate deposits to ocean temperature change, *Journal of Geophysical Research*, *113*, C12023, doi:10.1029/2008JC004938.

Reagan, M. T., and G. J. Moridis (2009), Large-scale simulation of methane hydrate dissociation along the West Spitsbergen Margin, *Geophysical Research Letters*, *36*, L23612, doi:10.1029/2009GL041332.

Reagan, M. T., G. J. Moridis, S. M. Elliott, and M. Maltrud (2011), Contribution of oceanic gas hydrate dissociation to the formation of Arctic Ocean methane plumes, *Journal of Geophysical Research*, *116*, C09014, doi:10.1029/2011JC007189.

Sarkar, S., C. Berndt, A. Chabert, D. G. Masson, T. A. Minshull, and G. K. Westbrook (2011a), Switching of a paleo-ice stream in northwest Svalbard, *Quaternary Science Reviews*, *30*, 1710-1725, doi: 10.1016/j.quascirev.2011.03.013.

Sarkar, S., A. Chabert, C. Berndt, T. A. Minshull, G. K. Westbrook, D. Klaeschen, and D. G. Masson (2011b), Seismic evidence for shallow fluid-escape features, offshore western Svalbard, *In*: *Proceedings of the Seventh International Conference on Gas Hydrates*, *Edinburgh*, *17-21 July*, *2011*.

Sarkar, S., C. Berndt , T.A. Minshull , G.K. Westbrook, D. Klaeschen , D. Masson, A. Chabert and K.E. Thatcher (2012), Seismic evidence for shallow gas-escape features associated with a retreating gas hydrate zone offshore west Svalbard, *Journal of Geophysical Research*, *117*, B09102, doi:10.1029/2011JB009126.

Shakhova N., I. Semiletov, I. Leifer, A. Salyuk, P. Rekant, and D. Kosmach (2010a) Geochemical and geophysical evidence of methane release over the East Siberian Arctic Shelf. *Journal of Geophysical Research*, *115*, C08007, doi:10.1029/2009JC005602.

Shakhova N., I. Semiletov, A. Salyuk, V. Yusupov, D. Kosmach and Ö. Gustafsson, (2010b) Extensive methane venting to the atmosphere from sediments of the East Siberian Arctic Shelf. *Science*, *327*, 1246-1250.

Sloan, E.D. and C.A. Koh, (2008), Clathrate Hydrates of Natural Gases, 3rd Edition, Taylor & Francis/CRC Press.

Spielhagen, R. F., K. Werner, S. A. Sorensen, K. Zamelczyk, E. Kandiano, G. Budeus, K. Husum, T. M. Marchitto, and M. Hald (2011), Enhanced modern heat transfer to the Arctic by warm Atlantic water, *Science*, *331*, 450, DOI: 10.1126/science.1197397.

Stone, H. L. (1970), Probability model for estimating three-phase relative permeability, *Trans. SPE AIME*, *249*, 214– 218.

Sultan, N., Cochonat, P., Canals, M., Cattaneo, A., Dennielou, B., Haflidason, H., Laberg, J.S., Long, D., Mienert, J., Trincardi, F., Urgeles, R., Vorren, T., Wilson, C., 2004. Triggering mechanisms of slope instability processes and sediment failures on continental margins: a geotechnical approach. *Mar. Geol.*, *213*, 291–321.

Sultan, N., V. Riboulot, V. Lanfumey, S. Ker, B. Marsset, L. Geli, J.-B. Tary, F. Klingelhoefer, M. Voisset, J. L. Colliat, J. Adamy, and S. Grimaud (2011), Dynamics of fault-fluid-hydrate system around a shale-cored anticline in deepwater Nigeria, *Journal of Geophysical Research*, *116*, B12, doi:10.1029/2011JB008218, 2011

Thatcher, K., and G. K. Westbrook (2011), Timing of methane release from hydrate dissociation on the west Svalbard margin, *in Proceedings of the 7th International Conference on Gas Hydrate*s, 17-21 July 2011, Edinburgh, Scotland, United Kingdom.

Van Genuchten, M. T. (1980), A closed-form equation for predicting the hydraulic conductivity of unsaturated soils, *Soil Sci. Soc. Am. J. 44*, 892– 898.

Vanneste, M., C. Berndt, J. S. Laberg, and J. Mienert (2007), On the origin of large shelf embayments on glaciated margins - effects of lateral ice flux variations and glacio-dynamics west of Svalbard, *Quaternary Science Reviews*, *26*, 2406-2419.

Walczowski, W., and J. Piechura (2007), Pathways of the Greenland Sea warming, *Geophys. Res. Lett.*, *34*, L10608, doi:10.1029/2007GL029974.

Westbrook, G.K., Chand, S., Rossi, G., Long, C, Bünz, S., Camerlenghi, A., Carcione, J.M., Dean, S., Foucher, J.P., Flueh, E., Gei, D., Haacke, R.R., Madrussani, J., Mienert, J., Minshull, T.A., Nouzé, H., Peacock, S., Reston, T., Vanneste, M., Zillmer, M. 2008. Estimation of gas-hydrate concentration from multi-component seismic data at sites on the continental margins of NW Svalbard and the Storegga region of Norway, *Marine and Petroleum Geology*, *25*, 744–758, doi:10.1016/j.marpetgeo.2008.02.003.

Westbrook, G. K., K. E. Thatcher, E. J. Rohling, A. M. Pitrowski, H. Pälike,, A. Osborne, E. G. Nisbet, T. A. Minshull, M. Lanoisellé, R. H. James, V. Hühnerbach, D. Green, R. E. Fisher, A. J. Crocker, A. Chabert, C. T. Bolton, A. Beszczynska-Möller, C. Berndt, and A. Aquilina (2009), Escape of methane gas from the seabed along the West Spitsbergen continental margin, *Geophysical Research Letters*, *36*, L15608, doi:10.1029/2009GL039191.

Yousif, M. H., H. H. Abass, and E. D. Sloan (1991), Experimental and theoretical investigation of methane-gas-hydrate dissociation in porous media, *SPE Reservoir Eng.*, *6*, 69– 76.